AEROACOUSTICS OF OSCILLATING AIRFOIL UNDER ICING CONDITIONS

Osman GUNGOR, Turkish Aerospace Industries/Middle East Technical University, Ankara, TURKEY
Taylan CAKIROGLU, Turkish Aerospace Industries, Ankara, TURKEY
Alper EZERTAS, Turkish Aerospace Industries, Ankara, TURKEY
Serkan OZGEN, Middle East Technical University, Ankara, TURKEY
Yusuf OZYORUK, Middle East Technical University, Ankara, TURKEY

Abstract

Ice accumulation on airfoil shapes changes the airfoil shape significantly depending on the severity of icing conditions. In rotor blades, blade profile goes under oscillation motion in forward flight. The shape change due to ice accumulation affects aerodynamic performance of the oscillating rotor blade and may risk the flight safety. Shape change of profile also affects pressure variation over the blade therefore acoustic signature is expected to change. In order to investigate possible use of acoustic signature change due to ice accretion, oscillating airfoil analyses are conducted with iced and clean profiles using Ffowcs Williams-Hawking approach. Acoustic pressure changes and frequency content are investigated. Significant sound pressure levels changes are observed at a specific frequency range at the one and two chord length distances. Sound energy is integrated at receiver locations. Comparison of sound energy for iced and clean profiles shows increasing trend with ice accumulation. Furthermore, the effect of exposure time on noise generation is explored. Horn formation is observed to change sound energy levels significantly. Changes in aerodynamic characteristics are resulted to be in line with noise generation.

1. NOTATION

Symbols

p_0	Reference pressure, Pa
c	Speed of sound, m/s
ρ	Air density, kg/m3

Acronyms:

RANS	Reynolds Averaged Navier Stokes
URANS	Unsteady RANS
SBES	Stress-Blended Eddy Simulation
LES	Large Eddy Simulation
DDES	Delayed Detached Eddy Simulation
MVD	Mean Volumetric Diameter
LWC	Liquid Water Content
SPL	Sound Pressure Level

2. INTRODUCTION

Icing can impact the performance of rotor blades and safety of flight, therefore detecting the presence of ice accretion could be benefical for ensuring safe flight operations. Accumulation of ice changes the shape of the profile therefore pressure field generated by the blades also changes. Variations in pressure field result in change of characteristics of noise generated by the blades. Hence, variations in acoustic signature may clue the accumulation of ice on blades. In literature, there are studies focused on the relationship between acoustic signatures and icing on airfoils, with researchers using high-fidelity simulations and experimental tests to investigate the effects of icing on the flow field and acoustic response.

One such study, conducted by Akbal et al. [1], used RANS, SBES, and LES to simulate the flow field and FENSAP-ICE for icing simulations, and found that iced airfoils generated a strong wake, causing pressure fluctuations and thickening of the boundary layer, which led to an increase in sound pressure levels at high frequencies. Another study, conducted by Zhou et al. [2], used the Spalart-Allmaras DDES approach to simulate the flow field and the FW-H approach for acoustic analyses, and found that iced airfoils generated significant wake structures, which led to an increase in sound pressure levels at high frequencies.

Icing wind tunnel test campaign conducted with collaboration of rotorcraft industry, NASA, and academia is selected as a valuable validation dataset for flow predictions and icing analyses [3, 4]. Tests were performed in the Icing Research Tunnel at NASA Glenn Research Center and focused on icing of oscillating airfoils, which were designed to mimic the motion of a rotor blade in forward flight conditions. Patented profile, SC2110, was used in the tests [5].

In the present work, aero-acoustic analyses of oscillating airfoil with ice accumulation are performed to explore whether acoustics signature can be used to detect ice accumulation. Variation of noise around the airfoil is investigated at different azimuthal and radial positions. Change of noise levels is examined at different exposure times.

3. MODELLING

The aero-acoustic analyses are conducted using StarCCM+ commercial software. URANS methodology with Spalart-Allmaras turbulence model with wall function approach is utilized for flow solution. Curvature correction for turbulence model is activated. Ffwocs-William Hawkings methodology is used for acoustic calculations. An inner cylindrical domain including airfoil surface and an outer cylindrical domain encapsulating the inner domain is generated. The inner domain oscillates while outer domain stays stationary. The information change between domains is achieved by sliding mesh interfaces. The airfoil surface is modelled as no-slip wall. Side walls of the domains are treated as symmetry. Boundary conditions are visualized in Figure 1. It should be noted that farfield is located at distance of 50 chords from airfoil surface however scaled down in Figure 1 for presentation purposes.

Icing analyses are performed with FENSAP commercial software. Unsteady icing analyses are started from a steady solution without any droplet trajectory calculation. Total exposure time is divided into equal time intervals for ice shape calculations. At each shot, 300 time steps are used with 5 inner iterations. After each shot, surface mesh and roughness is updated with automated scripts. Ice water model is selected as glaze ice and beading is activated.

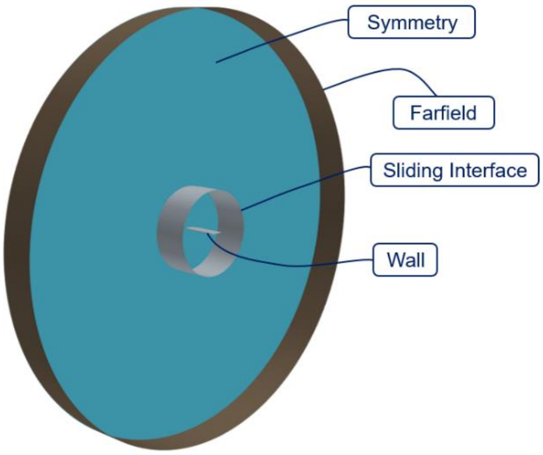

Figure 1 Oscillating Airfoil Model and Boundary Conditions

Quadrilateral elements are utilized on the airfoil surface as shown in Figure 2. Leading edge of the airfoil is discretized with fine elements in order to capture ice shape and high flow gradients. The element sizes on the leading and trailing edge is 0.005c while maximum element size on airfoil surface is 0.025c. Solution domain is discretized with polyhedral elements. First wall height distance is adjusted such that wall y+ value of 30 and higher is obtained over the airfoil surface with 5 layers of quadrilateral elements. Mesh refinement is applied around the airfoil geometry in a cylindrical region. On the sliding mesh interface boundary layer treatment is applied with thick cells in order to improve interpolation algorithm between two domains. Section views from the volume mesh are presented in Figure 3.

Oscillatory motion mandates the use of unsteady model. Second order implicit time stepping is utilized with 20 inner iterations. Algebraic multi grid method is also enabled with a V-cycle of maximum 30 levels.

(a) Leading Edge

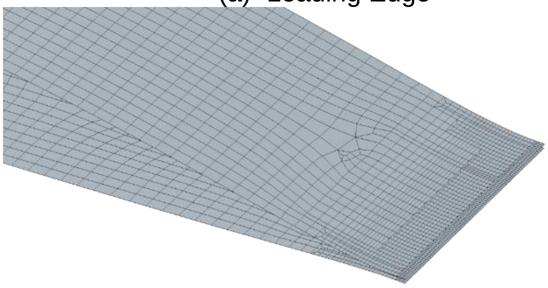

(b) Trailing Edge

Figure 2 Surface Mesh of Iced Airfoil (a) Leading Edge, (b) Trailing Edge

(a) Leading Edge

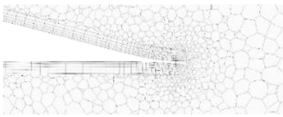

(b) Trailing Edge

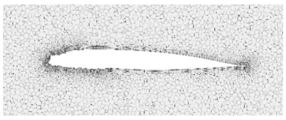

(c) Airfoil Nearfield

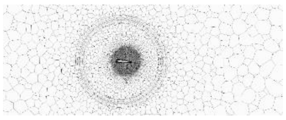

(d) Refinement

Figure 3 Volume Mesh, (a) Leading Edge, (b) Trailing Edge, (c) Airfoil Nearfield and (d) Refinement Region

4. RESULTS

4.1. Flow Solution for Oscillating Airfoil

Flow field and aerodynamic characteristics predictions under oscillatory motion are validated using wind tunnel test results available in literature. Aerodynamic characteristics of iced and clean airfoils are investigated in a special test run during oscillating airfoil icing tests in NASA Glenn Research Center [4]. The test condition represents a typical motion of a rotor blade in forward flight. SC2110 airfoil is tested under icing conditions while having oscillatory motion. The resultant ice shape is manufactured with a solid material for further testing. The aerodynamic performance of clean and iced airfoils are reported and used for validation purposes. The test conditions are given in Table 1.

Table 1 Testing Conditions for Icing Effect on Airfoil Performance *[4]*

Icing Conditions			
Temperature	-14 C	LWC	0.5 g/m3
MVD	22 µm	Chord	0.381 m
Oscillatory Motion			
Amplitude	3 deg	Mean Angle	5 deg
Frequency	2.8 Hz	Air Speed	150 Kts

The ice shape obtained from the test point given in Table 1 is provided in Figure 4. The clean and iced airfoils are modelled for specified test conditions. Simulation results are compared with test results in Figure 5. The lift coefficient values are presented in hidden axis. However, it is still useful to compare lift hysteresis and its change with ice accumulation. Clean airfoil has a stall-free hysteresis while iced profile has slight stall behavior and reduced lift generation capability. Simulation results show same findings of test. Stall behavior of iced profile is predicted harsher in the simulations.

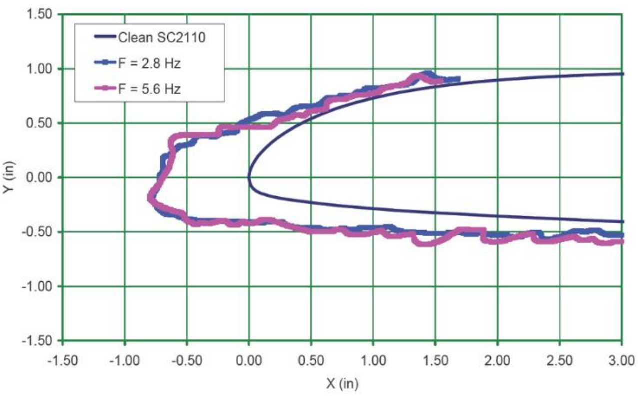

Figure 4 Ice Shape Obtained under Conditions Given in Table 1 *[4]*

Velocity magnitude contours of clean and iced profiles are compared in Figure 6. Clean airfoil experiences attached flow even at the highest angle of attack however iced profile is having large vorticity generation over upper surface implying flow separation. Separated flow of iced profile re-attaches at around 6 degrees. It is expected to have flow separation with iced profile due to its irregular shape on the leading edge.

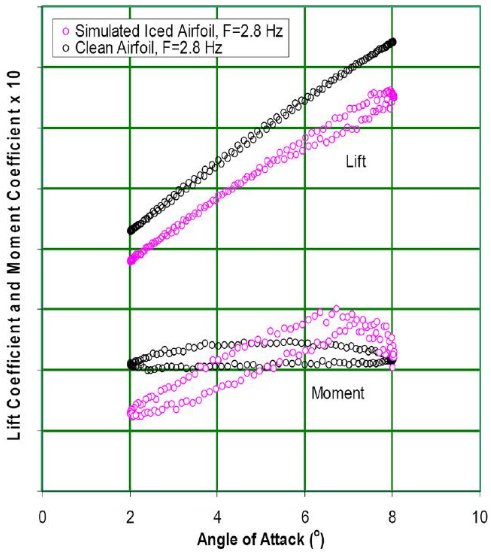

(a) Wind Tunnel Data

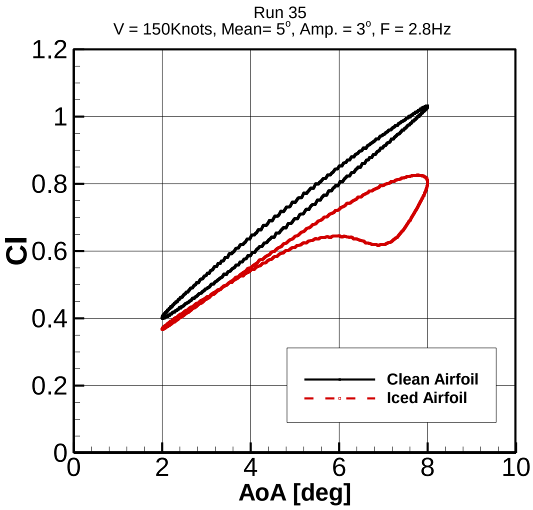

(b) Simulation Results

Figure 5 Lift Variation for Clean and Iced Airfoil, (a) Wind Tunnel Data *[4]*, (b) Simulation Results

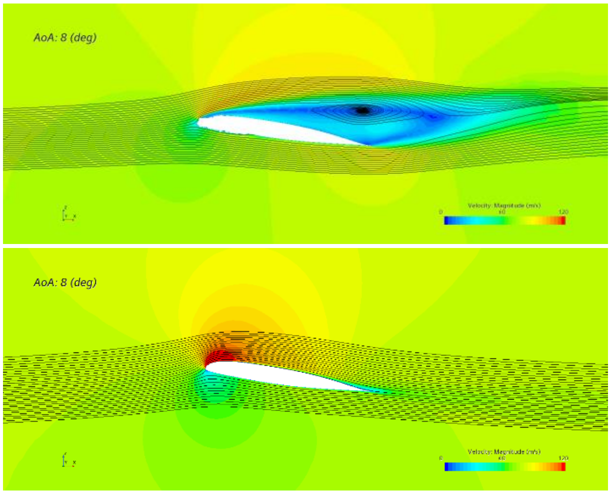

Figure 6 Velocity Magnitude Contours for Iced(Upper) and Clean Airfoil(Lower) at 8 Degrees Angle of Attack

4.2. Icing Solution for Oscillating Airfoil

Icing analysis is conducted for the conditions designated as Run61 in oscillating airfoil icing test campaign [3, 4]. The conditions are tabulated in Table 2. The exposure time is 600s. Simulations are performed for 10 shots of each being 60s. After each shot, surface mesh is updated to predicted ice shape. The results of icing analyses are compared with test results in Figure 7. The ice shape is in reasonably good agreement with test data. The distinctive horn structure is captured although lower horn is predicted to be aft of the test result. Apart from final ice shape, ice shape after each shot is also shown. After third shot horn structure starts to develop according to simulations.

Table 2 Test Conditions for Icing Analysis *[3]*

Icing Conditions			
Temperature	-14 C	LWC	1.0 g/m3
MVD	22 µm	Chord	0.381 m
Oscillatory Motion			
Amplitude	6 deg	Mean Angle	5 deg
Frequency	2.8 Hz	Air Speed	150 Kts

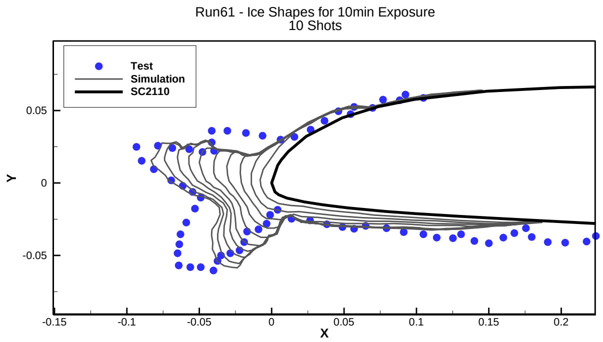

Figure 7 Ice Shape Predictions for Run61 and Comparison with Test Data

4.3. Acoustic Analyses for Oscillating Airfoils under Icing Conditions

Acoustic analyses are conducted for clean and iced airfoil for the conditions of Run61 defined in Table 2. Ice shape used in acoustic analyses is 10th shot of icing simulations. Duration of acoustic analyses are set for a total of 3 oscillation cycles. As depicted in Figure 8, acoustic receivers are located around the airfoil at different azimuthal and radial positions with respect to quarter chord position which is motion center.

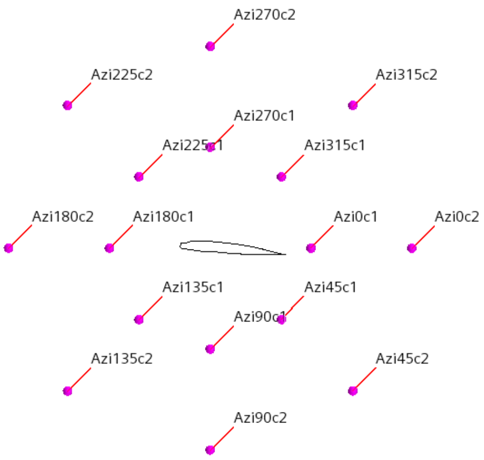

Figure 8 Acoustic Receivers around the Airfoil

Acoustic pressures variations with time is plotted in Figure 9, Figure 10, Figure 11 and Figure 12 for clean and iced profile at different azimuthal and radial locations. At all azimuthal locations, acoustic pressure variation synchronized with airfoil motion is observed for both clean and iced profile. Moreover, as the radial distance is increased, acoustic pressure values are observed to be decreased for both clean and iced profile. Azimuth 0 is located behind the trailing edge therefore it is expected to have minimum acoustic pressure change due to ice being accumulated on the leading edge. However, a change in mean acoustic pressure level and additional waveforms are observed with iced profile. At azimuth of 90, clean airfoil has a clear wave form, while iced profile having decrease in mean level and abrupt and periodic changes in acoustics pressure. Azimuth 180 shows a different characteristics at acoustics pressure variations. Change of mean values of iced and clean profile are more distinct compared to remaining azimuthal locations. Since the azimuth 180 is located upstream of the leading edge and leading edge is the point where ice is accumulated; effective surface is becomes closer to receiver with iced profile. Therefore, acoustic pressure levels are significantly increased compared to clean profile. Additional waveforms are also observed at azimuth of 180 with iced profile. At azimuth 270, similar changes are observed in acoustic pressure variations.

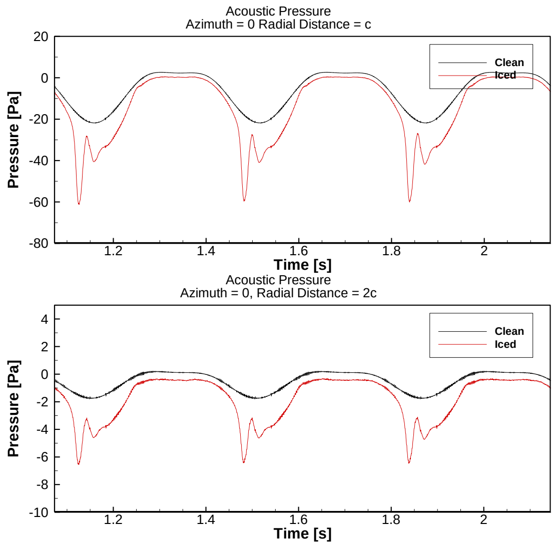

Figure 9 Acoustic Pressure for Azimuth 0

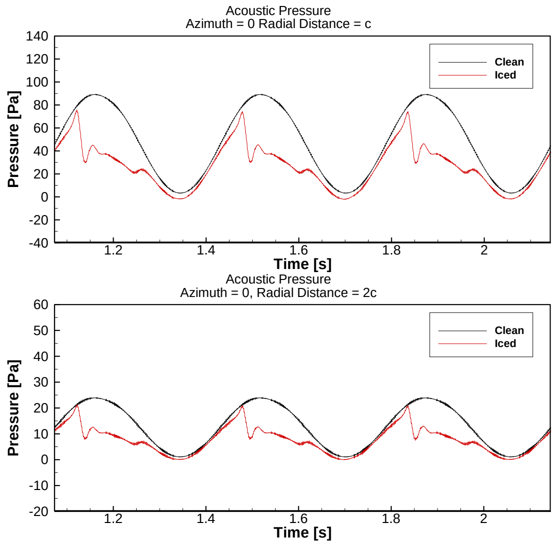

Figure 10 Acoustic Pressure for Azimuth 90

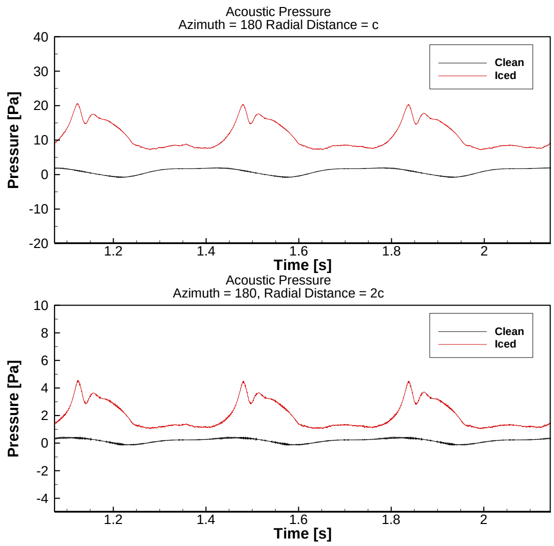

Figure 11 Acoustic Pressure for Azimuth 180

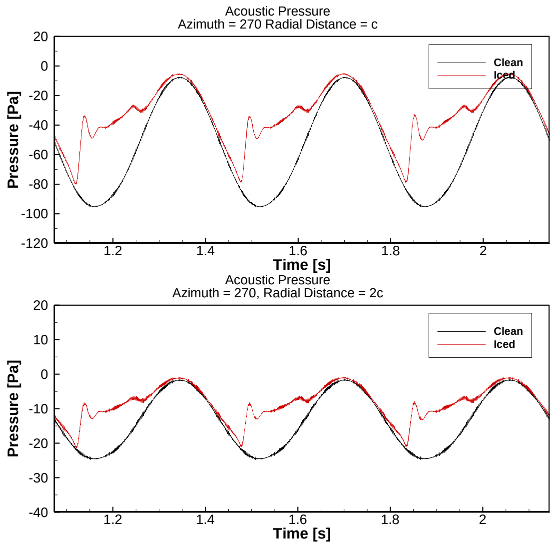

Figure 12 Acoustic Pressure for Azimuth 270

Frequency content of acoustic pressure is plotted in Figure 13 for azimuth 0 and radial location of one chord length. It is observed that sound pressure levels differ with clean and iced profile at low frequency values. High frequency content shows similar variations. Therefore, Figure 13 is plotted again for reduced range of frequency in Figure 14. Label ticks are arranged to multiples of oscillation frequency, 2.8Hz. Frequency content of azimuth 90, 180 and 270 are provided in Figure 15, Figure 16 and Figure 17, respectively. At all azimuth locations, sound pressure levels are increased. Moreover, sound pressure levels of iced profiles show distinct peaks at multiples of oscillation frequency. Similar to A-weighting approach in human perception of noise, a special weighting approach can be utilized for ice accretion detection with acoustic signature.

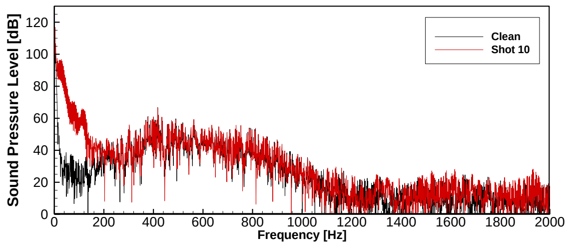

Figure 13 Frequency vs SPL for Azimuth 0, High Frequency Range

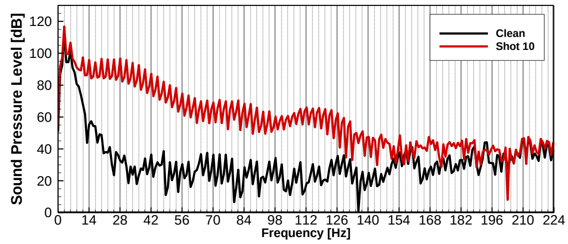

Figure 14 Frequency vs SPL for Azimuth 0

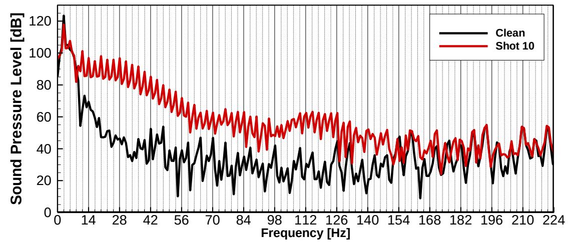

Figure 15 Frequency vs SPL for Azimuth 90

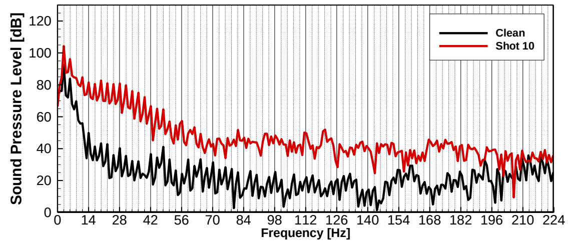

Figure 16 Frequency vs SPL for Azimuth 180

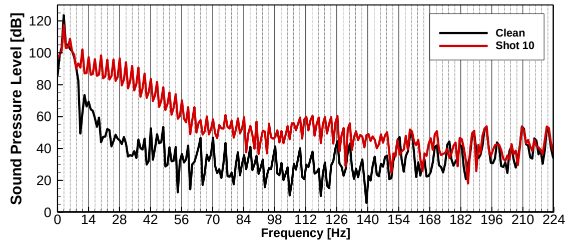

Figure 17 Frequency vs SPL for Azimuth 270

In order to compare the spatial variation of noise generated by clean and iced profile, Sound energy is calculated at receiver locations by integrating contribution of each frequency content. Reference energy value for sound energy is taken as ${p_0}^2/(\rho c)$. The comparison is given in Figure 18. Circles drawn at receiver locations are scaled with magnitude of sound energy. It is observed that sound energy reduces towards in the region of leading edge. Additionally, the sound energy levels decreased as the distance from the airfoil increased, which is consistent with theoretical formulations. The major conclusion is that sound energy integrated at all frequencies of clean and ice profiles are quite similar or clean profile has slightly more sound energy. When frequency content of sound pressure data is investigated, clean profile has higher sound pressure levels at motion frequency. It means that clean profile has higher loading noise and it can be observed from the lift hysteresis. Clean profile generates more lift compared to iced profile. Therefore, sound pressure magnitudes resultant from motion of airfoil are observed to be dominant in sound energy generation at very low frequencies.

Sound energy calculation is repeated at a frequency range of 14 Hz and 200 Hz to update the comparison as in Figure 19. Iced profile shows an increase in sound energy at all positions compared to clean profile with limited frequency range. It is concluded that ice accretion on airfoil causes noise increase at a certain frequency range with a decreasing trend around leading edge.

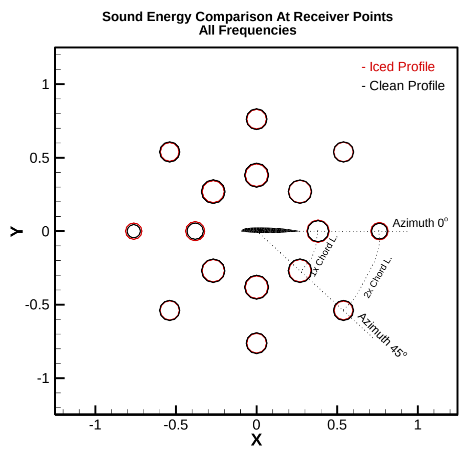

Figure 18 Sound Energy Comparison at Receiver Locations, All Frequencies

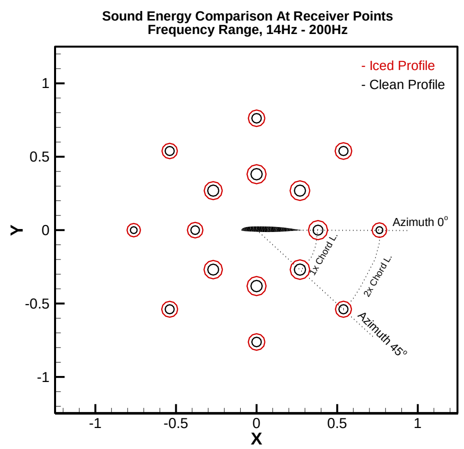

Figure 19 Sound Energy Comparison at Receiver Locations 14Hz – 200Hz Frequency Range

Figure 18 and Figure 19 compares clean and iced profile from shot 10 plotted in Figure 7. Aero-acoustic analyses of iced profiles at different exposure times are performed in order to observe the variation of noise levels with developing ice accumulation. Sound energy levels are plotted in Figure 20 for different exposure times at varying azimuthal locations. Exposure time for each shot is taken as 1 minute during icing analyses. In the figure, there are 4 sound energy levels at each azimuthal location. Each bar represents sound energy for profiles of clean, 1st, 5th and 10th shots. Ice profile at 1st shot is relatively smooth shape however, increase in sound energy is observed at all azimuth locations. From 1st shot to 5th shot, there is a significant jump in sound energy levels. The accumulated ice has developed a moderate horn shape at 5th shot. At 10th shot, horn shape almost doubles in size and becomes more irregular. Increasing trend continues with a slower rate. Similar to Figure 20, sound energy levels are plotted in Figure 21 for a 2 chord distance from the airfoil. As we expect, sound energy is reduced at all locations. Azimuthal distribution shows similar trend except for receiver at azimuth 0. At azimuth 0, sound energy drop with distance is resulted to be higher in magnitude compared to remaining receivers.

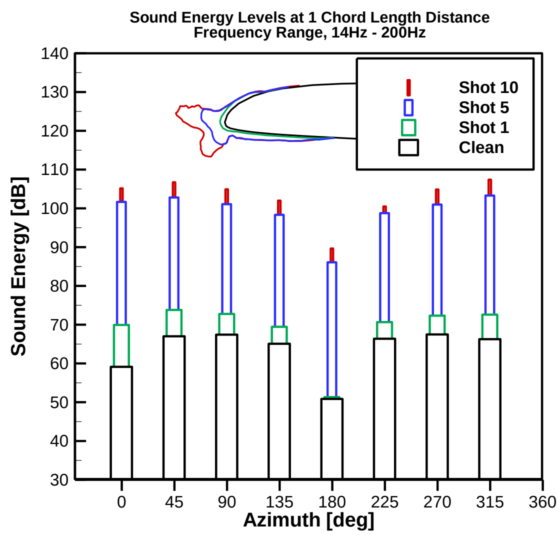

Figure 20 Sound Energy at 1 Chord Length Distance with Varying Azimuthal Location for Different Exposure Times

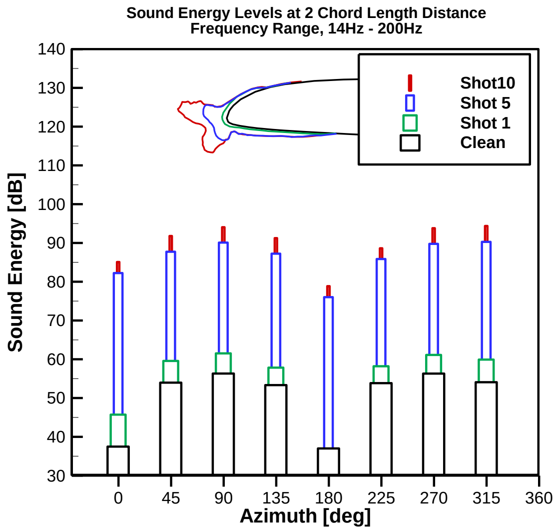

Figure 21 Sound Energy at 2 Chord Length Distance with Varying Azimuthal Location for Different Exposure Times

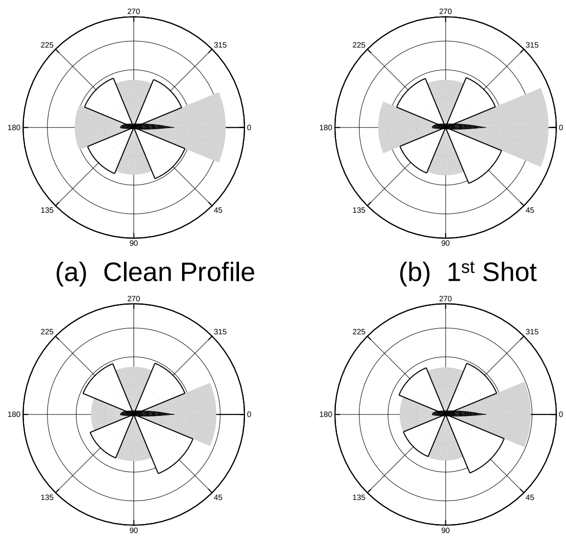

(a) Clean Profile (b) 1st Shot

(c) 5th Shot (d) 10th Shot

Figure 22 Sound Energy Reduction from 1 Chord Distance to 2 Chord Distance at Different Azimuthal Locations (a) Clean Profile, (b) 1st Shot, (c) 5th Shot and (d) 10th Shot

Sound energy drop variation with azimuthal directions is plotted in Figure 22 for different ice accumulation levels. For all profiles, maximum drop is observed at trailing edge direction. At the trailing edge, receiver at azimuth 0 is closer to airfoil surface therefore effective distance increase higher compared to remaining azimuth directions. Beside azimuth 0, azimuth 45 shows higher sound energy drop for all profiles.

The aerodynamic characteristics of clean and iced profiles are compared in Figure 23. Clean profile and 1st shot shows stall-free lift hysteresis while 5th and 10th shots are experiencing deep stall as expected due to large ice horns. Similar to lift, moment characteristics of iced profile shows abrupt changes. Variations in aerodynamic characteristics are in correlation with change of sound energy levels with accumulation of ice. In other words, as the ice accumulates, both the aerodynamics and the sound energy levels change in a connected way. Monitoring sound energy levels and vibratory data from blades or pitch link and combination of them might be used to detect ice accumulation.

It is important to note that lift capability of the profile is reduced by icing at different levels depending on the amount of ice accumulated. During the flight, iced blade has to generate same lift to sustain the flight. Therefore, loading noise is expected to increase for iced profiles. In other words, noise levels of iced profile has to elevate while providing same lift capability.

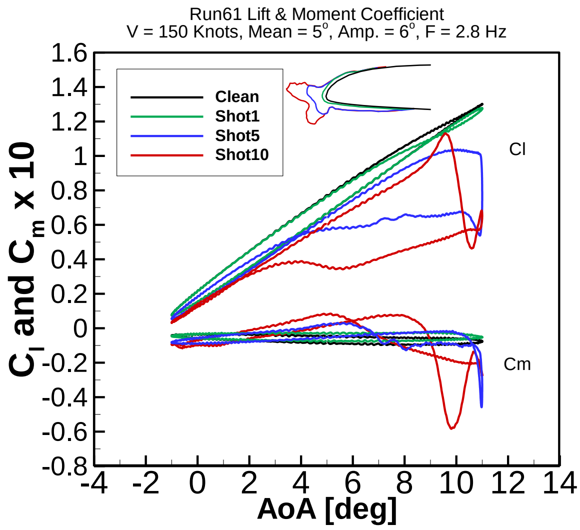

Figure 23 Lift and Moment Variation of Clean and Iced Airfoil

5. CONCLUSIONS

Ice accretion simulations with oscillating airfoils are performed and compared with test data. Ice shapes are captured reasonably well. The predictions of URANS solutions for aerodynamic characteristics are compared with limited test data and similar changes in lift variation are observed. The acoustics signature changes due to ice accumulation are investigated. Following conclusions are made:

1. Acoustic pressure and frequency content is observed to be affected by ice accumulation. Iced profiles show significant peaks in sound pressure

levels at multiples of oscillation frequencies. The overall change in sound pressure levels are resulted at low frequencies. However, it is important to note that flow solutions are obtained with URANS hence, repeating the analyses with higher fidelity methods is appointed as a future study to check high frequency content.
2. Sound energy is used as an integrated parameter to compare noise generation at receiver locations. Integrating sound energy for all frequencies resulted in almost no difference. However, a specific frequency range provided distinct variations between sound energy levels of iced and clean profiles.
3. Azimuth ±45, ±90 and ±135 directions are observed to radiating higher noise with ice accumulation. Azimuth 180 shows abrupt increase compared to remaining directions. It is probable that as the ice accumulates, effective distance reduces between receivers therefore noise increase becomes more sensible.
4. Sound energy levels decrease with increasing radial distance as in theoretical expectation. Sound energy levels drops more significant at trailing edge region. Since the center is taken as quarter chord location, receiver located at trailing edge region, azimuth 0, is closer to airfoil surface compared to receivers located at other azimuthal locations. It is possible that for receiver at azimuth 0, effective radial distance changes more than double compared to other locations.
5. Acoustic analyses were repeated for ice shapes resulted from varying exposure times. Formation of horn structure dramatically increased sound energy levels. After the horn structure is formed, sound energy level increase slows down.
6. Changes in aerodynamic characteristics are observed to be connected with noise characteristics. Horn structures cause to airfoil go under deep stall hysteresis and abrupt pitching moment changes. Hence, vibratory data can be used as supplementary data for acoustic ice detection.

Author contact:

Osman GÜNGÖR osman.gungor@tai.com.tr

6. REFERENCES

1. Akbal, Ö., Ayan, E., and Zafer, B., "A Case Study of Airfoil Aeroacoustic Characteristics in In-Flight Icing Conditions," *Ankara International Aerospace Conference*, Ankara, 2021.
2. Zhou, B. Y., Gauger, N. R., Morelli, M., Guardone, A., Hauth, J., and Huan, X., "Development of a Real-Time In-Flight Ice Detection System via Computational Aeroacoustics and Bayesian Neural Networks," *AIAA SciTech Forum*, Orlando, 2020.
3. Narducci, R., and Reinert, T., "Calculations of Ice Shapes on Oscillating Airfoils," *SAE International*, 2011.
4. Reinert, T., Flemming, R. J., Narducci, R., and Aubert, R. J., "Oscillating Airfoil Icing Tests in the NASA Glenn Research Center Icing Research Tunnel," *SAE International*, 2011.
5. Owen, S. J., "Airfoil for a Helicopter Rotor Blade," United States Patent US 2007/0187549 A1, 16 August 2007.